J. Chem. Sci. (2020)132:2
https://doi.org/10.1007/s12039-019-1691-9

REGULAR ARTICLE

First principles investigation on the applicability of ruthenium as a potential ORR catalyst

SURAJIT NANDI[a], AKHIL S NAIR[a] and BISWARUP PATHAK[a,b,*]
[a]Discipline of Chemistry, Indian Institute of Technology Indore, Simrol, Indore, Madhya Pradesh 453 552, India
[b]Discipline of Metallurgy Engineering and Materials Science, Indian Institute of Technology Indore, Simrol, Indore, Madhya Pradesh 453 552, India
E-mail: biswarup@iiti.ac.in

MS received 22 May 2019; revised 8 July 2019; accepted 3 August 2019

Abstract. Exploration of new materials for oxygen reduction reaction has long been a major area of research in heterogeneous catalysis. As the currently available oxygen reduction catalysts have not achieved the optimal efficiency, search for alternative resources is a continuing effort. Realizing the wide acceptance of ruthenium as a promising catalyst for various catalytic reactions, we have investigated the plausibility of Ru to perform in the bulk as well as nanoparticle forms as an efficient oxygen reduction reaction catalyst. Two nanoclusters with face-centred and hexagonal symmetry were scrutinized for ORR activity along with Ru(111) and Ru(0001) surfaces as periodic counterparts and compared the activity with Pt(111) surface. We report here that Ru cannot be an alternative to the Pt-based catalysts owing to a high overpotential.

Keywords. Oxygen reduction reaction; ruthenium catalysis; ruthenium nanoclusters; overpotential.

1. Introduction

Oxygen reduction is the main cathode component reaction of proton exchange membrane (PEM) fuel cells. The quest for the industrial-scale application of fuel cell reaction to act as alternative energy resources is very old although an expected advancement has not been achieved in this direction due to the slow kinetics of the ORR.[1–3] The oxygen reduction reaction (ORR) occurs at the cathode which reduces molecular O_2 to H_2O with two possible parallel pathways. Till date, Pt emerges as the most effective metal to efficiently catalyse the ORR. However, the high cost and low abundance of Pt enforces us to either constantly search for alternative options or reduce the Pt loading in the catalyst design. Many studies have been made in this direction to obtain alternative cathode material. To reduce the Pt loading, different strategies are used, e.g., designing Pt nanostructures, alloying Pt with other low-cost metals,[4–8] using core shell models,[9–11] and so on. Those models generally lack stability in the fuel cell environment and both the Pt and the other constituent metals tend to dissolve in the electrolyte solution. Hence, in recent years, enormous efforts have been given to try for different morphologies of various materials.[12]

The search for a better ORR catalyst has also driven towards the discovery of new metals for equivalent if not better catalytic activity relative to Pt. In this endeavour, different metals have been investigated either in its pure form or by alloying with metals. Pd,[13,14] Au,[15,16] Ag,[17,18] and Ni[19] clusters are shown to be very effective to catalyse the oxygen reduction in their pure form. Ruthenium has been identified as an efficient catalyst for various reactions of industrial and commercial importance for decades. These include the hydrogen evolution reaction,[20,21] carbon monoxide oxidation,[22] electrochemical water splitting,[23] catalytic oxidation of organic compounds and so on.[24] Se doped Ru nanoparticles are even experimentally tested for their feasibility as catalysts in direct methanol fuel cell (DMFC).[25,26]

Hexagonal close-packed (hcp) structure is the most stable phase of bulk Ru. The (0001) facet is known to

*For correspondence

Electronic supplementary material: The online version of this article (https://doi.org/10.1007/s12039-019-1691-9) contains supplementary material, which is available to authorized users.

Published online: 19 December 2019

be the most stable facet for bulk Ru and widely studied for its catalytic activity. A number of studies have been done by Stolbov and his co-workers on the hcp structure of Se modified Ru on the (0001) surface.[27–29] The authors also studied oxygen and hydroxyl adsorption on Ru(0001) along with the Se modified Ru surface.[29] Beside the naturally occurring hcp Ru, a face-centred cubic variant has recently been synthesised in nanoscale by reduction of $Ru(acac)_3$ and hydrated $RuCl_3$ with various sizes.[30] From powder X-ray diffraction study, it is detected that the (111) facet is the most abundant surface for fcc Ru nanoparticles of all the sizes. After its discovery, the stability of the nanoparticles from fcc Ru and its alloy forms have been investigated theoretically.[31,32] Despite the less stability of Ru fcc nanoparticles, Fang *et al.*,[33] were able to synthesize capped octahedral structure to study the catalysis for dehydrogenation reaction.[34] Recently, its utility for dehydrogenation reaction,[33] ammonia borane hydrolysis,[34] Fischer-Tropsch synthesis,[35] and hydrogen evolution reaction[36] has been studied by various research groups. Moreover, a recent study indicated very high ORR activity of Ru NC supported on nitrogen-doped graphene at elevated temperature.[36]

These efficient synthetic strategies and application to a number of electrocatalytic reactions indicate a possible broader scope of Ru for its potential application as ORR catalyst in a different type of fuel cells. To the best of our knowledge, no theoretical study has been reported for the ruthenium surfaces with a complete description of adsorption behaviour of intermediates and ORR analysis of energetics. Moreover, recent studies have shown that the activity of metal nanoclusters can be significantly different from that of their surface counterparts.[37–39] Henceforth, in the current study, we attempt to explore the plausibility of Ru in the periodic surface as well as in the nanoparticle form to examine the potential applicability of ruthenium as an ORR catalyst.

In this article, we report the activity of a model fcc Ru nanoparticle, a hcp Ru nanoparticle, periodic (3 × 3) slab model of fcc, and hcp Ru, for ORR. We consider a capped octahedron 79 atom nanocluster (NC) for which the stability has been analysed by cluster scaling technique by Soini *et al.*[40] For the hcp Ru, we have considered an 87 atom NC, for which the stability has been studied by Yusuke *et al.*[31] The two cluster models differ in the arrangement of low index facets and hence are expected to bring out variations in their catalytic activity. The observed activities are compared with Pt(111) periodic surface, the conventional ORR catalyst, to understand the plausibility of the emergence of Ru as an alternative to Pt-based catalysts.

2. Models and computational details

The Ru_{79} is comparable to the Pt_{79} nanocluster in structural aspects which has been well studied for its applicability for ORR in our group.[41] It has two facets, *viz.*, (111) and (001) separated by edge sites (Figure 1(a)). The Ru_{87} cluster has two different facets – one is the (0001) and another is $(10\bar{1}1)$. The geometry of the Ru_{87} NC is less symmetric compared to the Ru_{79} cluster. The (0001) facet has well defined and symmetric binding sites while the $(10\bar{1}1)$ facet does not have symmetric and well defined binding sites (Figure 1(b)). The $(10\bar{1}1)$ plane has a step-like structure where one row of Ru placed slightly below of the consecutive row. Spectroscopic data from experimental reports also show that the (0001) facet is the most exposed facet of all types of hcp Ru nanoparticles.[31] Hence we have focused on oxygen reduction occurring on the (0001) facet of the Ru_{87} NC. To compare the reactivity of the nanoparticles, we construct slab models for each of the fcc and hcp Ru.

Density functional theory (DFT) calculations are performed using a projector augmented wave (PAW)[42] method as implemented in the Vienna *ab initio* Simulation Package (VASP).[43–45] The exchange-correlation potential is described by using the generalized gradient approximation of Perdew–Burke–Ernzerhof (GGA-PBE).[46] A kinetic energy cutoff of 400 eV is used for all the calculations. The cutoff value of 400 eV was used previously to study oxygen adsorption over bulk Ru and it has been verified with sufficient accuracy.[28,29] A $25 \times 25 \times 25$ Å^3 cubic supercell is used to optimize the Ru_{79} nanocluster placed at the center to rule out the possibility of interactions between the periodically repeated clusters.

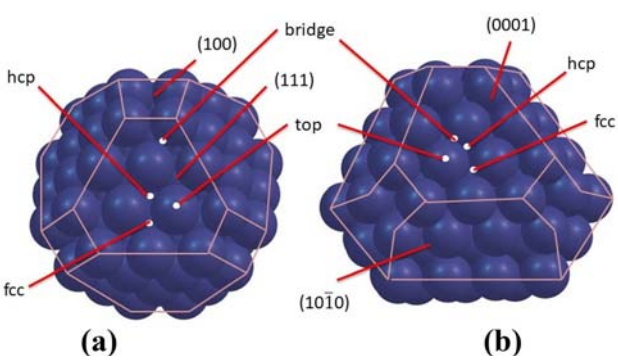

Figure 1. Structural models of (a) Ru_{79} and (b) Ru_{87} nanoclusters with facets and binding sites labelled.

During structural relaxation, all the atomic coordinates are optimized, whereas the cell volume and cell shape are kept fixed. The Brillouin zone is sampled with a gamma point (1 × 1 × 1) for clusters. The Ru(0001) and Ru(111) surface is modelled with a (3 × 3) supercell. The (3 × 3) is the minimum periodicity to be considered to diminish the lateral interactions between the repeating images. The metal slabs are composed of five atomic layers, where the bottom three layers are fixed and the top two layers are relaxed. A vacuum of 15 Å is used along the z-direction to avoid periodic interactions. The Brillouin zone is sampled using a 4 × 4 × 1 k-point grid for the surface calculations. All the systems are fully optimized, where the convergence criteria for total energy and forces are set at 10^{-4} eV and <0.02 eV $Å^{-1}$, respectively. Spin-polarized calculations are performed for all the molecular species and oxygen adsorbed intermediates. We have included Grimme's D3-type of the semiempirical method to incorporate the dispersion corrections to account the van der Waals interactions.[47] The binding energy (E_b) for all possible adsorbates are calculated using the following equation (I):

$$E_b = (E_* + E_{adsorbate}) - E_{*+adsorbate} \quad (I)$$

where, $E_{*+adsorbate}$ is the total energy of the surface+adsorbate, and E_* and $E_{adsorbate}$ are the single point energies of the surface and adsorbate in the optimized geometry of the surface + adsorbate, respectively. In this case, higher binding energy indicates stronger interaction. The adsorbed intermediate (R) is denoted with an asterisk (*) sign. The reaction free energies (ΔG) are calculated using the following equation (II),

$$\Delta G = \Delta E + \Delta ZPE - T\Delta S \quad (II)$$

where ΔE, ΔZPE and ΔS are the difference in total energies, zero-point energies and entropy between the product and reactant. The zero-point energy is calculated by using harmonic oscillator approximation, $ZPE = \sum_i \frac{1}{2} h\nu_i$, where h is Planck's constant and ν_i is the frequency of the i^{th} vibrational mode. The entropies of gas phase molecules are taken from ref. [49].

3. Results and Discussion

3.1 *Adsorption*

We have studied the adsorption only at the (111) facet of the Ru_{79} NC, and at the (0001) facet of the Ru_{87} cluster as these are the most prominent and catalytically active facets observed in similar studies. The possible binding sites for the intermediates on the clusters are represented in Figure 1. The binding modes of the ORR intermediates on Ru_{79} NC are given in Figure 2 and the binding energies of the most stable binding sites of Ru_{79}, Ru_{87} NCs, and Ru(0001) and Ru(111) periodic structures are given in Table 1. We have not considered the edge sites in the nanoclusters as such under-coordinated sites are expected to be strongly binding with ORR intermediate which leads to catalyst surface poisoning and hence a diminished ORR activity.[41]

The (111) facet of Ru_{79} has four possible binding sites, *viz.*, top, bridge, face-centred cubic (fcc) and hexagonal close-packed (hcp). The O_2 is stable only on top position with a binding energy of 1.11 eV. The optimization of the di-sigma adsorption leads to the breaking of the O–O bond. *O and *H are found to be most stable at the 3-fold hcp and fcc sites respectively, whereas bridge site is found to be the most stable for *OH and *OOH on the surface. It is to be noted here that the H atom of *OOH is directed inward after adsorption instead of sideways which is a common way of adsorbing OOH. The cluster offers a weak binding for H_2O (0.43 eV) and H_2O_2 (0.73 eV) similar to the Pt_{79} NC. The smaller binding energies observed for the product species H_2O and H_2O_2 remarks a favorable characteristic of ORR facilitating their easy desorption from the catalyst surface.

The O_2 binds in the periodic Ru(111) surface on two sites, *viz.,* top, and di-sigma with higher stability on top site with a binding energy of 1.02 eV. While *O and *OOH are found to retain their binding sites, the *OH species undergoes a change in binding site from the bridge to hcp while moving from Ru_{79} NC to Ru(111) surface. Furthermore, the H_2O and H_2O_2 are adsorbed relatively stronger on the Ru(111) surface with binding energies of 0.59 and 0.79 eV respectively. It is noteworthy that it is only the initial intermediate $*O_2$, which is adsorbed with a higher strength on Ru_{79} NC whereas all other intermediates of ORR are weakly bound on the Ru_{79} cluster as compared to Ru(111) surface which indicates a plausibility for enhanced ORR activity. This observation is slightly distinct compared to the ORR studies on Pt where the nanoclusters bind *O, *OH and *OOH intermediates much strongly than the periodic Pt(111) surface.[41]

The (0001) facet of the Ru_{87} NC also possesses four binding sites as well namely, top, bridge, fcc and hcp. Similar to the Ru_{79} NC, the O_2 prefers to adsorb on top with the binding energy of 1.07 eV. The most favourable binding sites for *O, *OH and *OOH are

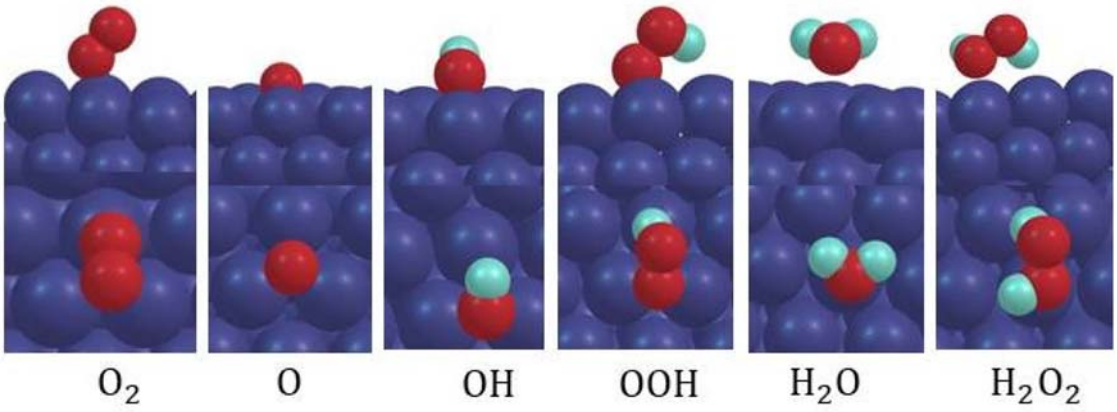

Figure 2. Binding modes of the reactants and intermediates involved in the oxygen reduction reaction on the (111) facet of the Ru_{79} NC.

Table 1. The binding energies (eV) of the ORR intermediate species with their most favourable binding sites (in parenthesis) on the (111) facet of Ru_{79}, (0001) facet of Ru_{97}, (0001) facet of periodic Ru(hcp), and (111) facet of periodic Ru(fcc). Here, b, d, f, h, and t refer to bridge, di-sigma, fcc, hcp, and top sites respectively.

Adsorbed Species	Ru_{79}	Periodic Ru(111)	Ru_{87}	Periodic Ru(0001)
$*O_2$	1.11(t)	1.02(t)	1.07(t)	3.71(d)
*O	6.07(h)	7.93(h)	6.20(h)	7.80(h)
*OH	3.43(b)	4.06(h)	3.58(h)	4.08(h)
*OOH	2.74(b)	3.20(b)	2.84(b)	2.99(b)
$*H_2O_2$	0.73(t)	0.79(t)	0.77(t)	0.83(t)
$*H_2O$	0.43(t)	0.59(t)	0.45(t)	0.63(t)
*H	2.85(f)	3.95(f)	2.92(f)	3.89(f)

found to be hcp, hcp and bridge sites respectively. By analyzing the binding energy values, it can be understood that all the intermediates are more strongly adsorbed on the Ru_{87} NC as compared to Ru_{79} NC. In the case of the periodic Ru(0001) surface, the $*O_2$ is stable only on the di-sigma position with considerably higher binding energy (3.71 eV) compared to other systems considered in this study. The adsorption behavior of all the ORR intermediates are exactly the same as in the case of Ru_{87} NC expect a high binding strength observed for H*. Similar to the Ru_{79} NC, a weakening of binding energies is also observed for Ru_{87} as well compared to its surface counterpart suggesting the constancy in adsorption trends irrespective of the crystalline nature (hcp and fcc) of ruthenium. It should be noted that the reported binding energy value of the *O and *OH on clean Ru(0001) are 6.25 and 3.55 eV respectively.[28] The difference in the binding energy values stems from the different theoretical levels and slab models used in the two studies. Also, the previous results did not include the dispersion correction and the bottom layers of the slab were not fixed which is necessary to model a metal surface. To confirm this claim, we further calculated the binding energy of *O for our slab model but without fixing the bottom two layers. Not surprisingly, we got the binding energy for O adsorption on the hcp site as 6.42 eV which closely resembles the reported binding energy of 6.25 eV given that we used dispersion correction over the DFT calculated total energy.

From the binding energy analysis, it is found that the adsorption of the ORR species shows some unique patterns which are unlike the much-studied Pt surface and nanocluster. The O_2 is stable only at the tilted position in case of the NCs. Any attempt to optimize the O_2 in di-sigma position led to breaking the molecule. Interestingly, the O_2 is only stable in the di-sigma position on periodic Ru(0001) whereas it is stable in both the top and di-sigma positions on periodic Ru(111). The intermediate *O prefers to bind in hcp site with the lowest binding energy for all the Ru systems that we have studied. The *OH is stable on the bridge site in Ru_{79} NC and in hcp site in all other cases. *OOH shows maximum stability when it binds on the bridge site in all cases with the maximum variation of the binding energy of $\approx$0.46 eV among the systems. A comparison with binding energies of ORR intermediates on Pt(111) surface (Table S1, Supplementary Information) suggests that all the

intermediates are much strongly adsorbed on the Ru systems. Interestingly, the Ru_{79} and Ru_{87} NCs show lesser deviation in binding strength from Pt(111) surface in comparison to the periodic Ru surfaces. The higher binding strength observed can be understood from the relatively less filled d bands of Ru(d^7s^1) in comparison to almost completely filled d bands of Pt(d^9s^1) which leads to greater stabilization of bonding states formed by the interaction with 2p orbitals of *O, and as well as *OH on Ru systems. The binding energy in all cases is higher in the periodic systems compared to the NCs which is perhaps the most intriguing fact in the Ru. In the case of *O, the binding energy difference even reach more than 1.5 eV. To explain the substantial increment of the binding energy of atomic oxygen, we calculated the strain for converting to the NCs. The Ru-Ru bond distance is 2.704, and 2.705 Å in the periodic Ru(0001), and Ru(111) respectively, which compresses to 2.618 Å, and 2.574 Å for Ru_{87} and Ru_{79} NCs. It corresponds to compressive strains of 3.2, and 4.8% for the Ru_{87} and Ru_{79} NCs respectively, with reference to the corresponding bulk Ru structure. A compressive strain enhances the Ru 4d-orbital overlapping and hence narrowing of d-band which weakens the adsorbate binding over the Ru clusters. Also, from the projected density of state analysis, (Figure 3), we found that the Ru 4d orbitals are more stabilized by interacting with the 2p orbitals of *O in case of the periodic structure compared to the NCs. Hence, the atomic oxygen binds more strongly on the slab (both hcp and fcc) than the nanoclusters.

3.2 *Overpotential calculation*

The activity of ORR catalyst can be determined by calculating the changes in free energy with the applied potential as proposed by Nørskov and co-workers.[48] Here, we have used the solvent correction model to calculate the free energy change for oxygen reduction. In the solvent corrected model, the free energies of the intermediates are modified upon the gas phase values by including the maximum number of H-bonds possible for a given intermediate. Hence, *OH, and *OOH are capable of forming two H-bonds each and they will be stabilized by the same order of magnitude.[49] In this scheme, the chemical reactions for the 4-electron reduction paths are given below (R1–R4).

$$O_{2(g)} + (H^+ + e^-) + * \leftrightarrow *OOH \quad (R1)$$

$$\Delta G_4 = (\Delta G_{OOH} - 0.30) + 2\Delta G_W \quad (III)$$

$$*OOH + (H^+ + e^-) \leftrightarrow *O + H_2O \quad (R2)$$

$$\Delta G_3 = \Delta G_O - (\Delta G_{OOH} - 0.30) \quad (IV)$$

$$*O + (H^+ + e^-) \leftrightarrow *OH \quad (R3)$$

$$\Delta G_2 = (\Delta G_{OH} - 0.30) - \Delta G_O \quad (V)$$

$$*OH + (H^+ + e^-) \leftrightarrow H_2O \quad (R4)$$

$$\Delta G_1 = -(\Delta G_{OH} - 0.30) \quad (VI)$$

In the above equations (III–VI), $2\Delta G_w$ is −4.92 eV which is the standard Gibbs free energy value of H_2O formation from H_2 and O_2. The Gibbs free energy value under the effect of applied potential is further calculated by the equation (VII).

$$\Delta G = \Delta E + \Delta ZPE - T\Delta S - eU \quad (VII)$$

Here ΔE is the changes in the electronic energy, ΔZPE is the change in zero-point energy, Δ*S* is the change in entropy and T is the absolute temperature, *e* is the transferred electronic charge after each reduction step, and *U* is the electrode potential generally considered against standard hydrogen electrodes. We have used a solvent correction of 0.30 eV to account for the enthalpy difference between gaseous and liquid water. According to the above equations, it is clear that the free energy of the water formation is mainly dependent on the free energy of formation of three key intermediates, *viz*., *OOH, *OH, and *O.

From Figure 4 and Table 2, it can be understood that the ORR energetics follows significant similarity between hexagonal derived Ru(0001) and Ru_{87} as well as cubic derived Ru(111) and Ru_{79} systems. In all the systems considered, it is *O and *OH reduction steps which are endergonic at the equilibrium potential of 1.23 V. This is exactly the trend observed for Pt(111) surface reported in previous studies.[36,50,51] Nevertheless, the overpotential is considerably high for Ru structures which are displayed in Figure 5 and compared with Pt(111) surface. The overpotentials for ORR are calculated as the free energy change (ΔG) associated with the highest endergonic elementary step at the equilibrium potential of 1.23 V as given in Table 2. A decrease in overpotential is observed for both Ru NCs considered in comparison to their surface counterparts with a higher difference (0.23 eV) between Ru_{79} and Ru(111) surface. In all the Ru based systems, it is *OH reduction (H_2O formation) which is the rate-determining step. Although this step has been identified as the rate-determining step for Pt(111) as well, all the Ru based catalyst systems are associated

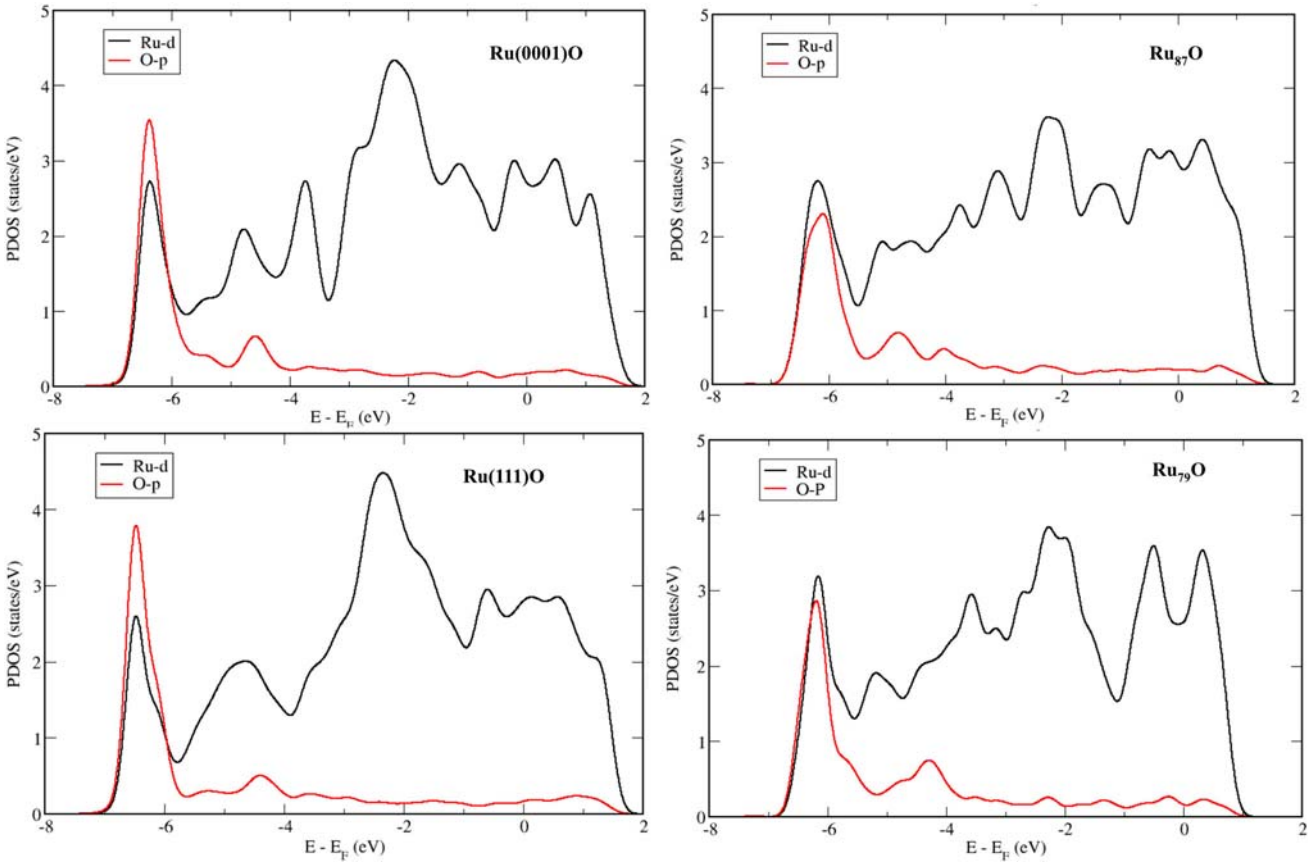

Figure 3. Projected density of state (PDOS) of *O on periodic Ru and Ru nanoclusters.

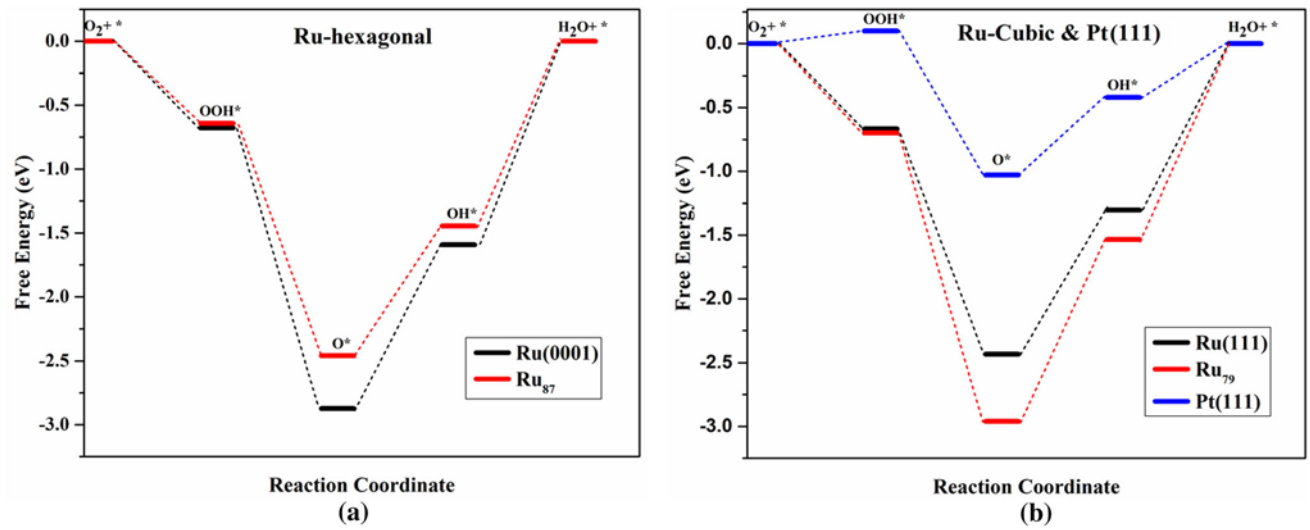

Figure 4. Solvent corrected free energy diagrams of the ORR mechanism at equilibrium potential of 1.23 V for (a) Ru_{87} and periodic Ru(0001) and (b) for Ru_{79}, periodic Ru(111) and periodic Pt(111).

with an overpotential more than double that observed for Pt(111) surface which suggests a diminished ORR activity for Ru compared to Pt. Nevertheless, the activity increment while moving from bulk to nanocluster regime is retained in Ru as well similar to that observed for Pt.[38,39]

It is noteworthy that while Ru(0001) and Ru(111) shows very much comparable overpotentials, the Ru NCs show a considerable difference in their activity with Ru_{79} NC showing the highest activity. The almost similar extent of ORR activities of Ru(111) and Ru(0001) surfaces can be understood from the similar

Table 2. The free energy change values (eV) and the overpotentials (V) associated with the elementary steps of ORR on the Ru_{87}, Ru(0001) periodic, Ru_{79}, Ru(111) and Pt(111) systems.

System	ΔG_1	ΔG_2	ΔG_3	ΔG_4	RDS	η_{ORR}
Ru_{87}	−0.64	−1.82	1.01	1.44	R4	1.44
Ru(0001)	−0.68	−2.19	1.28	1.59	R4	1.59
Ru_{79}	−0.66	−1.77	1.13	1.30	R4	1.30
Ru(111)	−0.70	−2.26	1.43	1.53	R4	1.53
Pt(111)	0.10	−2.03	0.61	0.42	R3	0.61

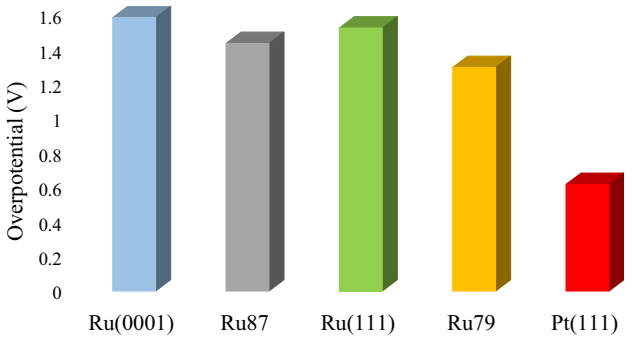

Figure 5. Overpotential comparison of considered Ru catalysts and Pt(111) surface.

*OH binding energy, interatomic distance and most favourable binding sites (hcp) for *OH adsorption. To rationalize the significantly differing activities for the Ru NCs with two different symmetries, we further scrutinize the binding energy of the intermediates. It is evident that the high overpotential is directly related to the free energy of formation of *O, and *OH over the surface of the catalyst which in turn depend on the binding energy of OH, O, and OOH. The negligible overpotential difference between Ru(0001) and Ru(111) surfaces can be attributed to their very close *OH binding energy of 4.06 and 4.08 eV, respectively. The Ru NCs owing to their lesser *OH binding energy (3.43 and 3.58 eV) allows the *OH reduction and it should exhibit a lesser surface poisoning by *OH species in comparison to the surfaces. Although, all these Ru systems show the high binding towards *O, the adsorption free energy difference $(\Delta G_O - \Delta G_{OH})$ is retained almost the same among all the systems with the maximum deviation of $\approx$0.2 eV among all, which hinders *OH formation from being the rate-determining step. In contrast with Pt(111) surface, Ru(111) and (0001) periodic structures are associated with exothermic O_2 reduction step owing to the lesser $*O_2$ binding energy and the binding pattern differences as well. The considerably high overpotential and hence reduced activity for Ru surface as well as NCs in comparison to Pt(111) which is the state of the art ORR catalysts arise from the increased binding strength towards the rate-determining intermediates *O, *OH and *OOH on Ru systems by the range of $\approx$1.5–3 eV. As it is generally accepted that Pt(111) itself over binds these intermediates and an optimal ORR activity can be expected when there is a slight weakening of binding (by 0.0–0.4 eV for *O and 0.0–0.2 eV for *OH) or a breaking of the scaling behavior of these intermediates, both Ru surface and NCs with high binding energy and retained scaling of intermediates are unable to outperform Pt(111) as ORR catalysts. Nevertheless, we have found out that the Ru(111) and Ru_{79} systems derived from the cubic crystalline structure show an improved catalytic activity as compared to those systems of hexagonal origin.

4. Conclusions

A systematic analysis of the ORR activity of Ru periodic surface and nanoclusters is performed. The adsorption study suggests all the Ru based systems considered exhibit strong binding to *O, *OH and *OOH intermediates in comparison to Pt(111) surface. Both Ru_{87} and Ru_{79} NCs offer less binding to the intermediates in comparison to their periodic counterparts. The electronic analysis shows this difference originates from the larger overlap between the Ru 4d orbital and the O 2p orbital in the periodic surface compared to the NCs. Free energy analysis has shown that all the Ru-based systems are associated with very high overpotential in comparison with the Pt(111) surface arising from the surface site-blocking owing to strong binding of intermediates on the catalyst surface. For all the Ru-based catalysts considered, H_2O formation is found to be the rate-determining step. An improvement in ORR activity while moving from bulk Ru surface to nanoclusters is observed which would trigger a further exploration of Ru-based nanoclusters for diverse electrocatalytic reactions. It was also evident from our study that the difference in symmetry of the NC surface of Ru_{87}, and Ru_{79}, leads to a slight improvement in ORR activity. Among all the pure Ru based systems considered, Ru_{79} NC is observed as the highest active catalyst with the least overpotential. Our work reports that Ru neither in the periodic surface nor in the nanocluster forms, outperform Pt(111) surface, which is the conventional ORR catalyst.

Supplementary Information (SI)

Table S1 containing binding energies of ORR intermediates on Pt(111) surface is available at www.ias.ac.in/chemsci.

Acknowledgement

We thank IIT Indore for providing the laboratory/computational facilities and DST SERB (Grant EMR/2015/002057) and CSIR (Grant 01(2886)/17/EMR-II) projects for funding. S.N. and A.S.N thank the Ministry of Human Resources and Development, India for research fellowship.

Compliance with ethical standards

Conflict of interest The authors declare no conflict of interest.

References

1. Jiao Y, Zheng Y, Jaroniec M and Qiao S Z 2015 Design of electrocatalysts for oxygen- and hydrogen-involving energy conversion reactions *Chem. Soc. Rev.* **44** 2060
2. Katsounaros I, Cherevko S, Zeradjanin A R and Mayrhofer K J J 2014 Oxygen electrochemistry as a cornerstone for sustainable energy conversion *Angew. Chem. Int. Ed.* **53** 102
3. Song C and Zhang J 2008 Electrocatalytic oxygen reduction reaction. In: *PEM fuel cell electrocatalysts and catalyst layers: fundamentals and applications* J Zhang (Ed.) (London: Springer) p. 89
4. Xu Y, Ruban A V and Mavrikakis M 2004 Adsorption and dissociation of O_2 on Pt−Co and Pt−Fe alloys *J. Am. Chem. Soc.* **126** 4717
5. Stamenkovic V R, Fowler B, Mun B S, Wang G, Ross P N, Lucas C A and Marković N N 2007 Improved oxygen reduction activity on $Pt_3Ni(111)$ via increased surface site availability *Science* **315** 493
6. Stamenkovic V, Mun B S, Mayrhofer K J J, Ross P N, Markovic N M, Rossmeisl J, Greeley J and Nørskov J K 2006 Changing the activity of electrocatalysts for oxygen reduction by tuning the surface electronic structure *Angew. Chem.* **118** 2963
7. Tang, W, Zhang L and Henkelman G 2011 Catalytic activity of Pd/Cu random alloy nanoparticles for oxygen reduction *J. Phys. Chem. Lett.* **2** 1328
8. Holewinski A, Idrobo J C and Linic S 2014 High-performance Ag-Co alloy catalysts for electrochemical oxygen reduction *Nat. Chem.* **6** 828
9. Wang, J X, Inada H, Wu L, Zhu Y, Choi Y, Liu P, Zhou W P and Adzic R R 2009 Oxygen reduction on well-defined core−shell nanocatalysts: particle size, facet, and Pt shell thickness effects *J. Am. Chem. Soc.* **131** 17298
10. Oezaslan M, Hasché F and Strasser P 2013 Pt-based core–shell catalyst architectures for oxygen fuel cell electrodes *J. Phys. Chem. Lett.* **4** 3273
11. Mazumder V, Chi M, More K L and Sun S 2010 Core/Shell Pd/FePt nanoparticles as an active and durable catalyst for the oxygen reduction reaction *J. Am. Chem. Soc.* **132** 7848
12. Sui S, Wang X, Zhou X, Su Y, Riffat S and Liu C J 2017 A comprehensive review of Pt electrocatalysts for the oxygen reduction reaction: nanostructure, activity, mechanism and carbon support in PEM fuel cells *J. Mater. Chem. A* **5** 1808
13. Erikson H, Sarapuu A, Tammeveski K, Solla-Gullón J and Feliu F M 2011 Enhanced electrocatalytic activity of cubic Pd nanoparticles towards the oxygen reduction reaction in acid media *Electrochem. Commun.* **13** 734
14. Lee C L and Chiou H P 2012 Methanol-tolerant Pd nanocubes for catalyzing oxygen reduction reaction in H_2SO_4 electrolyte *Appl. Catal. B* **117** 204
15. Chen W and Chen S 2009 Oxygen electroreduction catalyzed by gold nanoclusters: strong core size effects *Angew. Chem. Int. Ed.* **48** 4386
16. Jayabharathi C, Kumar S S, Kiruthika G V M and Phani K L N 2010 Aqueous CTAB-assisted electrodeposition of gold atomic clusters and their oxygen reduction electrocatalytic activity in acid solutions *Angew. Chem. Int. Ed.* **49** 2925
17. Chatenet M, Genies-Bultel L, Aurousseau M, Durand M and Andolfatto F 2002 Oxygen reduction on silver catalysts in solutions containing various concentrations of sodium hydroxide – comparison with platinum *J. Appl. Electrochem.* **32** 1131
18. Spendelow J S and Wieckowski A 2007 Electrocatalysis of oxygen reduction and small alcohol oxidation in alkaline media *Phys. Chem. Chem. Phys.* **9** 2654
19. Goubert-Renaudin S N S and Wieckowski A 2011 Ni and/or Co nanoparticles as catalysts for oxygen reduction reaction (ORR) at room temperature *J. Electroanal. Chem.* **652** 44
20. Drouet S, Creus J, Collière V, Amiens C, Garcí-a-Antón J, Sala X and Philippot K 2017 A porous Ru nanomaterial as an efficient electrocatalyst for the hydrogen evolution reaction under acidic and neutral conditions *Chem. Commun.* **53** 11713
21. Jiang P, Yang Y, Shi R, Xia G, Chen J, Su J and Chen Q 2017 Pt-like electrocatalytic behavior of Ru–MoO2 nanocomposites for the hydrogen evolution reaction *J. Mater. Chem. A* **5** 5475
22. Strebel C, Murphy S, Nielsen R M, Nielsen J H and Chorkendorff I 2012 Probing the active sites for CO dissociation on ruthenium nanoparticles *Phys. Chem. Chem. Phys.* **14** 8005
23. Tee S Y, Lee C J J, Dinachali S S, Lai S C, Williams E L, Luo H -K, Chi D, Hor T S A and Han M Y 2015 Amorphous ruthenium nanoparticles for enhanced electrochemical water splitting *Nanotechnology* **26** 415401
24. Baguc I B, Celebi M, Karakas K, Ertas I E, Keles M N, Kaya M and Zahmakiran M 2017 Nanohydrotalcite supported ruthenium nanoparticles: highly efficient heterogeneous catalyst for the oxidative valorization of lignin model compounds *ChemistrySelect* **2** 1019
25. Johnston C M, Cao D, Choi J H, Babu P K, Garzon F and Zelenay P 2011 Se-modified Ru nanoparticles as ORR catalysts: Part 2: Evaluation for use as DMFC cathodes *J. Electroanal. Chem.* **662** 257

26. Choi J H, Johnston C M, Cao D, Babu P K and Zelenay P 2011 Enhancement of activity of PtRh nanoparticles towards oxidation of ethanol through modification with molybdenum oxide or tungsten oxide *J. Electroanal. Chem.* **662** 267
27. Stolbov S 2010 First-principles study of formation of Se submonolayer structures on Ru surfaces *Phys. Rev. B* **82** 155463
28. Stolvob S 2012 Nature of the selenium submonolayer effect on the oxygen electroreduction reaction activity of Ru(0001) *J. Phys. Chem. C* **116** 7173
29. Zuluaga S and Stolbov S 2012 First principles studies of the size and shape effects on reactivity of the Se modified Ru nanoparticles *J. Phys.: Condens. Matter*. **24** 345303
30. Kusada K, Kobayashi H, Yamamoto T, Matsumura S, Sumi N, Sato K, Nagaoka K, Kubota Y and Kitagawa H 2013 Discovery of face-centered-cubic ruthenium nanoparticles: facile size-controlled synthesis using the chemical reduction method *J. Am. Chem. Soc.* **135** 5493
31. Nanba Y, Ishimoto T and Koyama M 2017 Structural stability of ruthenium nanoparticles: a density functional theory study *J. Phys. Chem. C* **121** 27445
32. Xiong Z, Wang X, Cao L, Wang J, Yu J, Yin H, Wang X and Mao J 2017 Structural stability, phase transition, electronic, elastic and thermodynamic properties of RuX (X = Si, Ge, Sn) alloys under high pressure *J. Alloy. Compd.* **693** 440
33. Fang Y, Li J, Togo T, Jin F, Xiao Z, Liu L, Drake H, Lian X and Zhou H C 2018 Ultra-small face-cantered-cubic Ru nanoparticles confined within a porous coordination cage for dehydrogenation *Chem* **4** 555
34. Alyami N M, LaGrow A P, Anjum D H, Guan C, Miao X, Sinatra L, Yuan D J, Mohammed O F, Huang K W and Bakr O M 2018 Synthesis and characterization of branched fcc/hcp Ruthenium nanostructures and their catalytic activity in ammonia borane hydrolysis *Cryst. Growth Des.* **18** 1509
35. Li W Z, Liu J X, Gu J, Zhou W, Yao S Y, Si R, Guo Y, Su H Y, Yan C H, Li W X, Zhang Y W and Ma D 2017 Chemical insights into the design and development of face-centered cubic Ruthenium catalysts for Fischer–Tropsch synthesis *J. Am. Chem. Soc.* **139** 2267
36. Ye R, Liu Y, Peng Z, Wang T, Jalilov A S, Yakobson B I, Wei S-H and Tour J M 2017 High performance electrocatalytic reaction of hydrogen and oxygen on ruthenium nanoclusters *ACS Appl. Mater. Interfaces* **9** 3785
37. Demir E, Akbayrak S, Önal A M and Özkar S 2017 Nanoceria-supported Ruthenium(0) nanoparticles: highly active and stable catalysts for hydrogen evolution from water *ACS Appl. Mater. Interfaces* **10** 6299
38. Wang Y-J, Long W, Wang L, Yuan R, Ignaszak A, Fang B and Wilkinson D P 2018 Unlocking the door to highly active ORR catalysts for PEMFC applications: polyhedron-engineered Pt-based nanocrystals *Energy Environ. Sci*. **11** 258
39. Miyazaki K and Mori H 2017 Origin of high oxygen reductionreaction activity of Pt12 and strategy to obtain better catalystusing sub-nanosized Pt-alloyclusters *Sci. Rep.* **7** 45381
40. Soini T M, Ma X, Aktürk O U, Suthirakun S, Genest A and Rösch N 2016 Extending the cluster scaling technique to ruthenium clusters with hcp structures *Surf. Sci.* **643** 156
41. Mahata A, Rawat K S, Choudhuri I and Pathak B 2016 Cuboctahedral vs. octahedral platinum nanoclusters: insights into the shape-dependent catalytic activity for fuel cell applications *Catal. Sci. Technol.* **6** 7913
42. Blochl P E 1994 Projector augmented-wave method *Phys. Rev. B: Condens. Matter Mater. Phys.* **50** 17953
43. Kresse G and Hafner J 1993 Ab initio molecular dynamics for liquid metals *Phys. Rev. B: Condens. Matter Mater. Phys.* **47** 558
44. Kresse G and Hafner J 1994 Ab initio molecular-dynamics simulation of the liquid-metal–amorphous-semiconductor transition in germanium *Phys. Rev. B: Condens. Matter Mater. Phys.* **49** 14251
45. Kresse G and Joubert D 1999 From ultrasoft pseudopotentials to the projector augmented-wave method *Phys. Rev. B: Condens. Matter Mater. Phys.* **59** 1758
46. Perdew J P, Chevary J A, Vosko S H, Jackson K A, Pederson M R, Singh D J and Fiolhais C 1992 Atoms, molecules, solids, and surfaces: applications of the generalized gradient approximation for exchange and correlation *Phys. Rev. B: Condens. Matter Mater. Phys.* **46** 6671
47. Grimme S, Antony J, Ehrlich S and Krieg S 2010 A consistent and accurate ab initio parametrization of density functional dispersion correction (DFT-D) for the 94 elements H-Pu *J. Chem. Phys.* **132** 154104
48. Nørskov J K, Rossmeisl J, Logadottir A, Lindqvist L, Kitchin J R, Bligaard T and Jonsson H 2004 Origin of the overpotential for oxygen reduction at a fuel-cell cathode *J. Phys. Chem. B* **108** 17886
49. Calle-Vallejo F, Martinez J I and Rossmeisl J 2011 Density functional studies of functionalized graphitic materials with late transition metals for oxygen reduction reactions *Phys. Chem. Chem. Phys.* **13** 15639
50. Li K, Li Y, Wang Y, He F, Jiao M, Tang H and Wu Z 2015 The oxygen reduction reaction on Pt(111) and Pt(100) surfaces substituted by subsurface Cu: a theoretical perspective *J. Mater. Chem. A* **3** 11444
51. Duan Z and Wang G 2013 Comparison of reaction energetics for oxygen reduction reactions on Pt(100), Pt(111), Pt/Ni(100), and Pt/Ni(111) surfaces: a first-principles study *J. Phys. Chem. C* **117** 6284